Geophys. J. Int. (2003) **153,** 133–145

Moment tensor inversion of recent small to moderate sized earthquakes: implications for seismic hazard and active tectonics beneath the Sea of Marmara

Ali Pinar,[1] Keiko Kuge[2] and Yoshimori Honkura[3]

[1] *Istanbul University, Engineering Faculty, Department of Geophysics* 34850, *Avcilar, Istanbul, Turkey. E-mail: alipinar@istanbul.edu.tr*
[2] *Kyoto University, Department of Geophysics, Kyoto* 606-8502, *Japan. E-mail: keiko@kugi.kyoto-u.ac.jp*
[3] *Tokyo Institute of Technology, Department of Earth and Planetary Sciences, Tokyo,* 152-8551, *Japan. E-mail: yhonkura@geo.titech.ac.jp*

Accepted 2002 October 15. Received 2002 October 15; in original form 2001 July 10

SUMMARY

We retrieve the moment tensors of 64 small to moderate sized events that occurred mostly beneath the Sea of Marmara using near-field data recorded at strong-motion and broad-band seismic stations. The near-field displacement records are inverted to their sources utilizing Kuge's method where the best fit between the synthetic and observed seismograms is achieved through searching a centroid moment tensor (CMT) point in a grid scheme. We also analyse the stress fields acting in the eastern and western parts of the Sea of Marmara by inverting the *P*- and *T*-axes of the focal mechanisms obtained. Significant biases in the stress tensors are obtained. The nearly horizontal maximum compressive axis σ_1 in the western part is rotated 16° counter-clockwise compared with σ_1 in the eastern part. The σ_2-axis is close to vertical (shear tectonic regime) in the east and the plunge of σ_2-axis in the west is 36° (transpressive tectonic regime). Changes in the σ_3-axis are also observed, that is, it is close to horizontal in the east and dips 49° in the west.

The spatial distribution of the focal mechanisms suggests that the stress field in the eastern part of the Sea of Marmara is homogenous compared with the western part, and we identify five distinct subsidiary faults. (1) a WNW–ESE-striking, right-lateral strike-slip fault located a few kilometres SW of the Princes' Islands, (2) a WSW–ENE-striking, right-lateral strike-slip fault named the Yalova–Hersek fault, (3) an E–W-striking normal fault located onshore between Yalova and Çinarcik, (4) a NNW–SSE-striking, left-lateral strike-slip fault located NE of the Princes' Islands and (5) minor thrust faults located in the Central High of the Sea of Marmara and in the vicinity of the Hersek Delta. The locations and the sense of motion of these five shear zones are explained by a very simple deformation model that requires a major E–W-striking right-lateral strike-slip fault, namely the North Anatolian Fault (NAF), within a stress field with maximum compression, σ_1, in the NW–SE direction and minimum compression, σ_3, in the NE–SW direction, as was derived from the stress tensor analysis. The mechanisms of the events occurring in the western part of the Sea of Marmara reveal a heterogeneous stress field that may result from the change in the strike of NAF from nearly E–W to WSW. The western Marmara Sea events are consistent with a deformation model that requires a major right-lateral strike-slip fault striking ENE–WSW with a stress field with maximum principal stress axis, σ_1, oriented ESE and minimum principal stress axis, σ_3, oriented NNE.

Key words: active tectonics, Marmara Sea, moment tensor inversion, seismic hazard.

1 INTRODUCTION

Recent GPS studies indicate that the rate of strain accumulation along the faults in the Sea of Marmara region is 22 ± 3 mm yr^{-1} (Straub *et al.* 1997; Kahle *et al.* 2000; McClusky *et al.* 2000). The historical and recent earthquake catalogues suggest that almost the whole accumulated deformation has been seismically released and major earthquakes are characteristic of the region (Ambraseys & Jackson 2000; Parsons *et al.* 2000). Two major events, one that occurred immediately to the west of the Sea in 1912 (M_s = 7.4) and a second that recently took place to the east of the Sea (M_w = 7.5), define the whole Marmara Sea as a seismic gap. The recently

determined GPS velocities rates and the fact that more than two centuries have passed since the previous major moment release clearly indicate that the seismic hazard potential has already drastically increased and encourages researchers to identify the faults beneath the Sea of Marmara so as to better assess the seismic hazard of the region (Smith *et al.* 1995; Wong *et al.* 1995; Okay *et al.* 1999, 2000; Parke *et al.* 1999; Imren *et al.* 2001).

Since only one moderate sized event (1963 Çınarcık earthquake, $M_s = 6.3$) has occurred beneath the Sea since the deployment of the Worldwide Standardized Seismograph Network (WWSSN), most studies of fault kinematics in the region are based on seismic reflection and/or bathymetry data. Imren *et al.* (2001) recently analysed multichannel seismic and multibeam bathymetry data and suggested that the region beneath the Sea is the subject of a shear tectonic regime. They further suggest that the North Anatolian Fault (NAF) crosses the Sea of Marmara as a continuous strike-slip fault system connecting the Izmit fault (IF) broken by the 1999 event with the Ganos fault (GF), broken by the 1912 event (Fig. 1a). According to their model, the three deep basins were formed earlier and are cut by the so-called Marmara fault, which is believed to accommodate most of the deformation west of Izmit fault.

Parke *et al.* (1999) acquired and analysed seismic reflection profiles and came to the conclusion that the three deep basins are located above the hanging walls of large normal faults that bound the basins in the north and the south and cross the sea in an east–west direction in an *en echelon* fashion.

Okay *et al.* (2000) added a few more multichannel reflection profiles to the data set of Parke *et al.* (1999) and re-interpreted the seismic cross-sections, concluding that strike-slip faulting is the dominant deformation pattern beneath the sea and the motion is mainly accommodated along two branches of NAF. The northern branch follows a trace similar to the Marmara fault of Imren *et al.* (2001) shaping the three deep basins and another bounding the southern shelf (Fig. 1b).

Siyako *et al.* (2000) reinterpreted 4300 km of seismic reflection profiles acquired by the Turkish petroleum organization, TPAO, and identified the whole Marmara Sea as a negative flower structure in its centre comprising a series of four offset right-lateral strike-slip fault segments connecting the Izmit segment of the NAF in the east with the Ganos fault in the west (Fig. 1c).

Smith *et al.* (1995) investigated the southern shelf, collecting very high-frequency shallow-penetrating sparker seismic profiles, and identified several active normal faults dipping north and striking nearly E–W. They also observed large displacements on some of these faults.

The seismic reflection study of Wong *et al.* (1995) shows two fault systems: one consists of two *en echelon* normal fault systems that bound the northern and southern shelves and the other consists of NE–SW right-lateral strike-slip faults and their conjugate NW–SE left-lateral strike-slip faults. These two fault systems divide the Sea of Marmara into five subsiding blocks: three deep pull-apart basins with higher subsidence rates separated by two push-up blocks (Fig. 1d). The slightly different tectonic model of Barka & Kadinsky-Cade (1988) also suggests that the three deep basins were formed as transtensional pull-apart basins (Fig. 1e).

In this study we retrieve moment tensors of 64 small to moderate sized events that occurred in the Sea of Marmara to complement existing information. As discussed above, there are several competing tectonic models. We believe that our moment tensor results will assist in discriminating amongst and perhaps even eliminating some of the present models of the tectonics acting beneath the Sea of Marmara. For example, although some models suggest that extensional tectonics should be dominant in the Çınarcık basin, we could not derive a single normal faulting mechanism among the several events analysed.

2 MOMENT TENSOR RETRIEVAL

No events of $M > 5.5$ have occurred in the Sea of Marmara since the installation of the WWSSN, except the 1963 September 18 Yalova–Çınarcık earthquake ($M_s = 6.3$). Therefore, the seismotectonics beneath the Sea of Marmara is still a matter of debate as discussed by Straub *et al.* (1997), Kalafat (1998), Siyako *et al.* (2000) and Gürbüz *et al.* (2000) and others in the previous section. Fortunately, during the previous decade, along with the deployment of three-component broad-band stations, near-field and regional moment tensor inversion methods have been developed and are widely used to recover the source parameters of small to moderate sized events (Fan & Wallace 1991; Dreger & Helmberger 1993; Singh *et al.* 1997; Delouis & Legrand 1999; Kuge 1999; Legrand & Delouis 1999; Legrand *et al.* 2000).

Recently, six broad-band seismic stations were installed around the Sea of Marmara (Fig. 2). We analyse seismic records from these stations to retrieve the faulting parameters of events occurring beneath and around the Sea of Marmara using the technique developed by Kuge (1999) and Ritsema & Lay (1995). In this method, waveform fitting between the observed and the synthetic displacement seismograms from one or more stations at local distances is achieved by searching for a CMT point on a grid scheme for which the best fit between the observed and the synthetic displacement seismograms is achieved. Because the events we analysed were located using a local seismic network, only the centroid depths were explored, though the method allows for a 3-D search. The synthetics are calculated following Kohketsu (1985) for a horizontally layered structure. We examined the crustal structure velocity models of Kalafat *et al.* (1987) and Gürbüz *et al.* (2000), correlated the observed arrival times with those predicted for *P* and *S* waves and found that the model of Kalafat *et al.* (1987) fits the observed *P* and *S* traveltimes more satisfactorily. For most of the events, the data were bandpass filtered between 0.04–0.1 Hz. Higher frequencies were used only for a few smaller events. Fan & Wallace (1991) showed that the waveforms in the low-frequency band are less sensitive to crustal models and that fault parameters can be successfully determined without knowledge of fine crustal structure.

During the inversion process we give uniform weight to all the seismograms. The quality of fit between the observed and predicted seismograms is measured by variance reduction (VR)—the larger the value of VR, the better the fit. The variance reduction is calculated for various depths and we select the faulting mechanism for which VR is the maximum as that of the analysed event. Fig. 3 shows an example of the results of a moment tensor inversion for broad-band records at six stations; however, in some cases, waveform data were available only at a smaller number of stations. For analyses of several events we used a three-component waveform data from a single station. There are several studies in the literature showing that three-component broad-band data from a single station can be used to retrieve a moment tensor reliably (Fan & Wallace 1991; Delouis & Legrand 1999; Dreger & Savage 1999; Kim & Kraeva 1999; Legrand & Delouis 1999). We performed a test to examine the reliability of the results obtained by inversion of waveforms at a single station, using the records of the 1999 August 31 ($M_w = 5.2$) event at ISK, an event for which a Harvard CMT is available. The results are shown in Fig. 4, which can be considered as an example

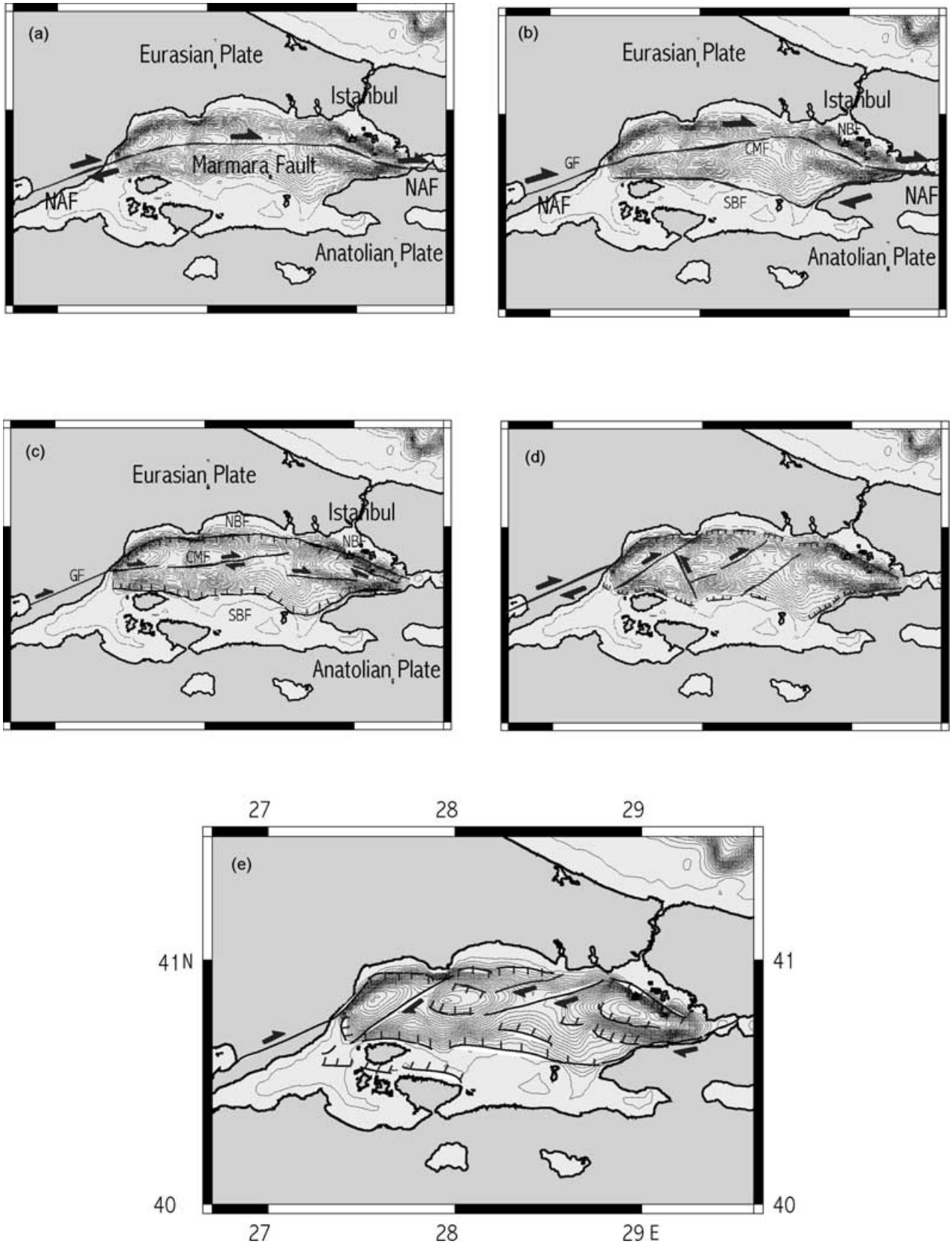

Figure 1. Tectonic models proposed by various investigators for the Sea of Marmara, (a) Imren *et al.* (2001), (b) Okay *et al.* (2000), (c) Siyako *et al.* (2000), (d) Wong *et al.* (1995), (e) Barka & Kadinsky-Cade (1988). The abbreviations are as follows: GF, Ganos fault; CMF, Central Marmara fault; SBF, southern boundary fault; NBF, northern boundary fault; NAF, North Anatolian fault; IM, Izmit fault. The arrows indicate the sense of motion. The contour interval for bathymetry is 50 m.

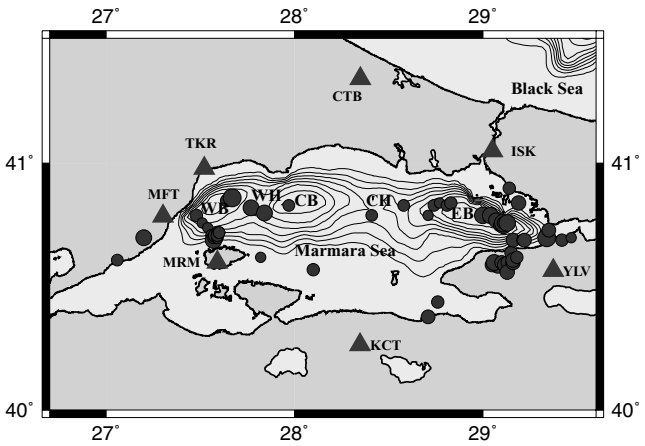

Figure 2. The locations of the events for which moment tensors are retrieved, shown by the solid circles. The broad-band seismic stations operated by Kandilli Observatory and Earthquake Research Institute (KOERI) are abbreviated as ISK, CTT, MRM, MFT, KCT and YLV, the locations and names of which are available in the international seismological centres. A CMG-3T seismometer is operated at station ISK and CMG-40Ts at the rest. TKR is the three component accelerometer deployed in Tekirdag and operated by the Earthquake Research Department of the Directorate of Disaster Affairs, Ankara: WB, western (Tekirdağ) basin; WH, western high; CB, central basin; CH, central high; EB, Eastern (Çınarcık) basin.

of a calibrated Green function for the eastern Marmara up to frequencies of 0.1 Hz and even higher. The amplitude and waveform fit between the observed and calculated seismograms and the similarity between our CMT solution and the independent Harvard CMT solution are perfectly good. These, in turn, suggest that our crustal structure model predicts the amplitude and phase of waveforms at station ISK; thus, three-component broad-band data at a single station can be successfully used in retrieving CMT of the events that occur in the eastern part of the Sea. Unfortunately, we could found no event to perform a similar calibration test for the western part of the Marmara.

We also checked the quality of the CMT solutions of smaller sized events by resampling the stations. Event 6 in Table 1 is one of the small events we analysed. Three-component broad-band records at stations MRM and MFT were available for this event. In many cases, for events of this size and smaller, only single-station three-component data were available and they were used to retrieve a moment tensor. To check the reliability of the moment tensors for such smaller sized events, we performed the following analysis in respect of Event 6: first, we obtained a CMT using the waveforms of both MRM and MFT stations. Then, we obtained two further CMT solutions for the same event, using only the records at MFT and using only the records at MRM station. The similarity of the resultant moment tensor for the three cases was satisfactory. Before concluding with the success of a single-station solution we should state that if the station is at the 'wrong azimuth', that is, close to nodal planes then certain fault parameters could be poorly resolved.

In addition to the six broad-band stations, data were available from the strong motion station deployed at Tekirdağ (TKR in Fig. 2), and we analysed four moderate sized events ($M_w > 4.5$) that occurred in the Tekirdağ Basin during 1995 and 1996.

Thus, in total we determined the moment tensor of 64 events, most of which took place following the 1999 Izmit earthquake ($M_w = 7.5$). The locations and the results are given in Fig. 5 and Table 1 shows the parameters of these events. Recently, Örgülü & Aktar (2001) analysed 10 of our 64 events using the same data set but a different technique. They used the regional moment tensor inversion method described by Dreger & Helmberger (1991, 1993) and obtained results that are similar to ours, even though they modelled only the longer periods.

3 REGIONAL STRESS TENSOR ANALYSIS

The method we use to derive the stress tensor acting on the faults in the Sea of Marmara is described by Gephart & Forsyth (1984), Gephart (1985, 1990). Our data are the orientation of the *P*- and *T*-axes of the fault plane solutions we determined. In the method, the earthquakes are assumed to have occurred in a region with no spatial or temporal changes in the stress field, and the associated slip direction is the shear stress direction on the fault plane. The method yields a stress tensor defined by the three principal stress components, namely, maximum compression, (σ_1), intermediate compression, (σ_2), minimum compression, (σ_3), and the stress magnitude ratio defined as $R = (\sigma_2 - \sigma_1)/(\sigma_3 - \sigma_1)$. The value of R is an indicator of the dominant stress regime acting in the region under investigation; $R = 0$ when $\sigma_1 = \sigma_2$ (biaxial deviatoric compression or state of confined extension), $R = 1$ when $\sigma_2 = \sigma_3$ (uniaxial deviatoric compression or state of confined compression) and $R = 0.5$ when $\sigma_1 = \sigma_2 = \sigma_3$ (*uniform triaxial compression*) (Christova & Tsapanos 2000). The combination of these four parameters (σ_1, σ_2, σ_3 and R) is called a stress model and the model that most closely matches the whole observed data set is called the best-fitting stress model. The best-fitting model is searched for in a grid over the four model parameters, systematically adjusting one at a time through a wide range of possibilities (Gephart 1990). The measure of misfit is given by the smallest rotation about an axis of any orientation that brings one of the nodal planes and its slip direction into an orientation consistent with the stress model (Slancova *et al.* 2000). Thus, for each stress model, the misfits between the orientation of the observed data and prediction are estimated and summed. The minimum misfit is the one that yields the smallest sum of misfits and is selected as the regional stress tensor for the region.

In our study, we start the inversion with an initial stress model close to that obtained by Pınar *et al.* (2001), with horizontal σ_1 and σ_3 compression axes striking 120° and 30°, respectively. A fine grid search with an increment of 5° is performed around the σ_1- and σ_3-axes to find the best stress tensor. Our data set includes 64 pairs of *P*- and *T*-axes derived in this study (Table 1). We performed the analysis using two data sets: (1) a subset of the data including only the events that occurred in the eastern part of the Sea of Marmara and (2) the same, but for the western part of the Sea of Marmara. The inversion yielded the following results: (1) for the data set including only the eastern Marmara Sea events the azimuth and plunge pairs for the three principal stress axes σ_1, σ_2 and σ_3 are 128°, 18°; 19°, 69°; 221°, 11°, respectively, and (2) for the data set including only the western Marmara Sea events the azimuth and plunge pairs for the three principal stress axes σ_1, σ_2 and σ_3 are 112°, 18°; 9°, 36°; 223°, 49°, respectively.

We show the stress inversion results for the data sets (1) and (2) in Fig. 6. The observed *P*- and *T*-axes distributions are given in Fig. 6(c); the quality of fit evaluated through the misfit measure and the area of the 95 per cent confidence limit are shown in Fig. 6(b); and the amplitude stress ratio diagram, R, is shown in Fig. 6(a).

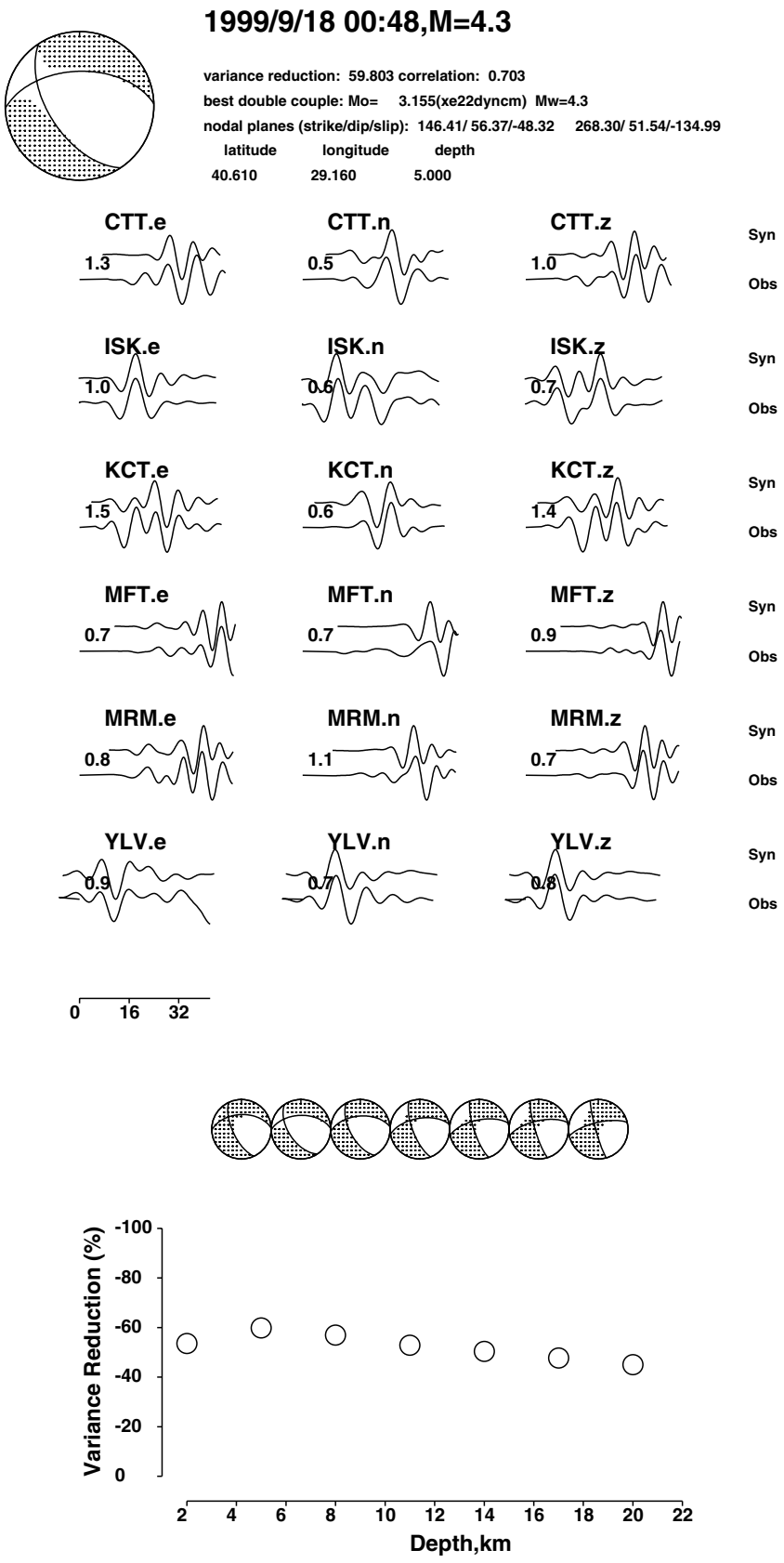

Figure 3. The moment tensor inversion result for the 1999 September 18 earthquake ($M_w = 4.3$) is illustrated as an example. The focal mechanism diagram is shown at the upper left, the source parameters are denoted to the right of the focal sphere, the synthetics (upper) and observed (lower) seismograms for east–west (e), north–south (n) and vertical (z) components at each station are shown along with the synthetic-to-observed ratio, the number between the two seismograms. The quality of the solution is given by the variance reduction versus depth plot at the bottom of the figure.

Table 1. Earthquake parameters and moment tensor inversion results of 64 events: H, depth in km; P_{az}, azimuth of the P-axis in degrees; P_p, plunge of the P-axis in degrees; T_{az}, azimuth of the T-axis; and T_p, plunge of the T-axis.

No	Date	Time	Lat.	Long.	H	M_w	Strike	Dip	Rake	P_{az}	P_p	T_{az}	T_p
1	16.11.1999	00 : 29	40.61	27.06	5	3.4	79	79	172	305	2	35	13
2	14.04.1996	08 : 30	40.70	27.20	12	4.6	274	61	−112	143	66	20	13
3	20.12.1999	22 : 35	40.79	27.48	11	3.6	99	65	−96	357	69	166	20
4	02.10.1999	11 : 28	40.76	27.51	8	3.0	272	75	170	138	4	229	18
5	24.09.1999	18 : 28	40.74	27.54	14	3.1	195	39	135	74	14	189	60
6	21.09.1999	01 : 09	40.71	27.56	5	3.4	224	75	168	90	2	181	19
7	21.09.1999	12 : 46	40.70	27.57	11	3.4	208	34	−42	208	58	84	19
8	20.09.1999	21 : 28	40.69	27.57	11	4.8	245	40	166	105	26	220	41
9	20.09.1999	20 : 36	40.70	27.57	11	3.3	246	51	156	115	13	216	42
10	03.12.1999	08 : 20	40.71	27.58	5	3.8	237	22	−139	40	56	185	29
11	07.10.1999	00 : 55	40.71	27.59	8	3.0	214	74	142	269	13	169	38
12	20.09.1999	21 : 44	40.70	27.59	5	3.2	211	50	138	89	5	187	55
13	21.09.1999	20 : 34	40.72	27.59	11	3.3	273	46	−168	123	37	232	23
14	20.09.1999	22 : 16	40.71	27.59	11	3.6	238	42	166	99	24	211	40
15	06.10.1999	06 : 59	40.72	27.60	14	3.2	208	46	139	85	9	189	56
16	20.09.1999	23 : 40	40.72	27.60	5	3.2	209	77	160	257	4	165	23
17	14.03.2001	20 : 34	40.85	27.64	17	3.7	75	79	147	127	14	29	31
18	13.04.1995	04 : 08	40.86	27.67	12	5.0	92	46	−137	291	57	34	8
19	08.02.1995	21 : 24	40.82	27.77	12	4.5	33	42	−137	226	58	335	12
20	18.04.1995	05 : 36	40.80	27.84	12	4.5	20	70	133	80	14	335	47
21	17.11.1999	19 : 14	40.83	27.97	11	3.4	276	82	132	335	25	223	38
22	22.09.1999	23 : 02	40.62	27.82	11	3.0	89	79	−163	313	20	222	4
23	23.08.1999	20 : 01	40.57	28.10	15	3.7	270	67	162	138	4	230	29
24	07.01.2000	01 : 48	40.79	28.41	5	3.2	283	77	−165	146	20	56	1
25	29.12.1999	12 : 26	40.83	28.58	14	3.4	98	27	132	337	23	115	60
26	29.05.1999	22 : 43	40.79	28.71	20	3.1	341	22	72	265	24	102	65
27	03.09.1999	04 : 18	40.83	28.74	5	3.2	353	70	19	305	1	214	27
28	21.08.1999	11 : 36	40.84	28.77	11	3.1	293	58	−143	147	47	237	1
29	21.08.1999	21 : 08	40.83	28.81	11	3.2	5	72	−40	321	41	61	12
30	24.03.2001	13 : 07	40.84	28.83	11	3.7	106	87	−160	332	16	239	12
31	17.08.1999	18 : 35	40.38	28.71	11	3.8	255	59	−169	113	29	211	14
32	17.08.1999	14 : 31	40.44	28.76	17	3.7	248	60	177	110	19	208	23
33	20.10.1999	23 : 08	40.79	29.00	8	4.9	32	71	16	345	3	254	24
34	17.08.1999	06 : 20	40.78	29.03	16	3.1	108	54	−175	325	28	67	21
35	17.08.1999	05 : 54	40.79	29.04	11	4.5	207	89	−7	162	6	252	4
36	17.08.1999	01 : 48	40.77	29.07	11	4.2	208	82	−27	163	25	259	13
37	18.08.1999	00 : 45	40.75	29.09	5	3.5	196	66	−18	156	29	64	5
38	17.08.1999	01 : 31	40.75	29.11	11	4.7	202	68	1	159	15	65	16
39	17.08.1999	01 : 33	40.76	29.11	11	5.2	112	88	170	158	6	67	8
40	17.08.1999	04 : 18	40.76	29.11	15	3.7	95	79	−177	319	10	50	6
41	17.08.1999	02 : 09	40.76	29.12	11	3.5	204	76	2	160	8	68	11
42	17.08.1999	04 : 14	40.76	29.13	13	4.7	105	82	163	152	6	60	18
43	16.01.2001	03 : 33	40.90	29.14	8	3.7	256	68	−163	117	27	209	4
44	07.07.2000	00 : 15	40.84	29.19	5	4.2	142	39	−32	128	52	13	18
45	19.08.1999	15 : 17	40.59	29.08	6	4.9	121	37	−66	138	72	14	10
46	20.08.1999	20 : 12	40.59	29.05	2	3.9	121	46	−65	109	72	14	2
47	19.08.1999	14 : 15	40.60	29.06	5	4.4	131	45	−61	121	70	21	4
48	19.08.1999	14 : 24	40.60	29.10	2	3.8	146	49	−56	125	65	33	1
49	20.08.1999	09 : 28	40.59	29.12	5	4.4	105	46	−56	91	66	352	4
50	28.08.1999	05 : 23	40.60	29.13	5	3.5	217	77	−161	81	23	349	4
51	31.08.1999	22 : 28	40.56	29.13	5	4.2	270	59	−105	144	72	11	13
52	19.08.1999	15 : 48	40.64	29.15	11	3.7	154	75	−45	106	42	212	17
53	22.08.1999	01 : 47	40.60	29.16	2	4.1	140	23	−77	206	67	40	22
54	18.09.1999	00 : 48	40.61	29.16	6	4.3	146	56	−48	114	56	208	2
55	20.08.1999	09 : 34	40.62	29.18	8	3.6	114	30	−41	119	58	349	22
56	09.09.1999	01 : 32	40.69	29.16	7	4.0	69	80	148	121	14	23	29
57	23.08.1999	22 : 36	40.69	29.21	14	3.4	65	36	178	277	34	36	36
58	23.08.1999	21 : 54	40.69	29.22	5	3.9	48	56	−168	264	31	4	16
59	31.01.2000	14 : 38	40.71	29.34	8	4.1	76	32	−149	262	52	28	24
60	29.09.1999	00 : 13	40.70	29.34	14	5.0	244	71	170	109	7	202	20
61	17.08.1999	14 : 27	40.73	29.35	11	3.2	356	49	86	89	4	231	85
62	17.08.1999	20 : 30	40.73	29.35	11	3.9	20	72	17	333	1	242	25
63	22.08.1999	08 : 23	40.69	29.42	8	3.6	354	84	−43	302	34	50	24
64	17.08.1999	11 : 29	40.70	29.47	5	3.1	342	20	25	303	34	159	50

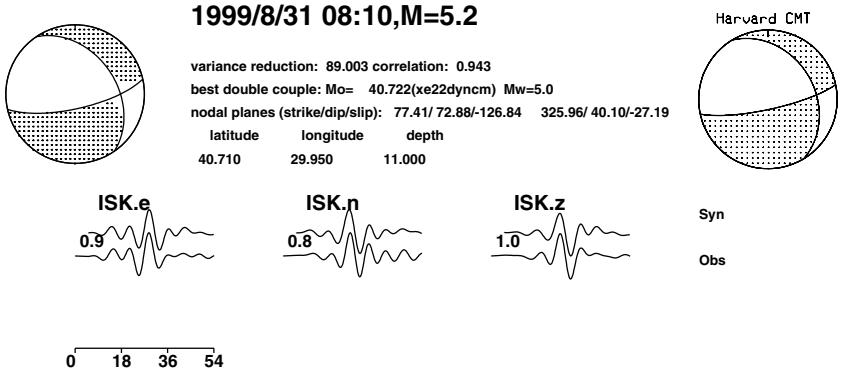

Figure 4. Moment tensor inversion using a single station three-component broad-band data. The moderate sized aftershock ($M_w = 5.2$) of the 1999 Izmit earthquake ($M_w = 7.5$) which occurred at 08:10 (GMT) on 1999 August 31 and was recorded at ISK station is used for analysis. Harvard centroit moment tensor (CMT) for this event is available and compared with the result obtained using the single-station data. For explanations, see the figure caption for Fig. 3.

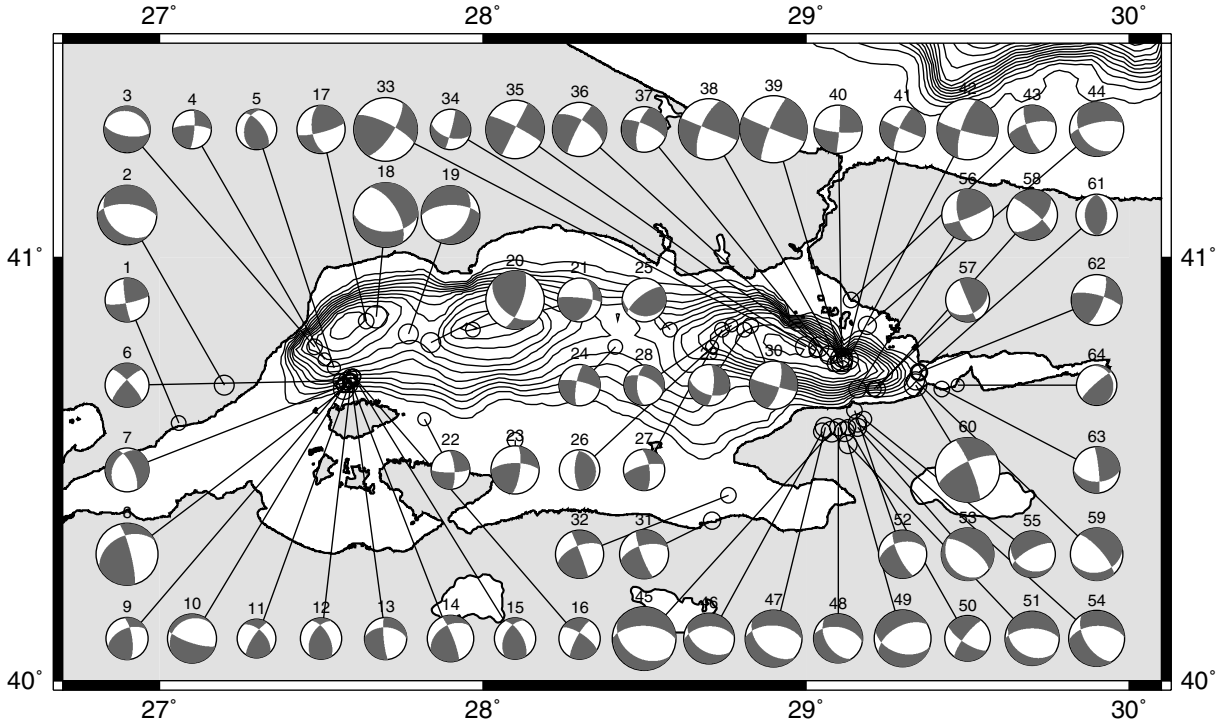

Figure 5. The locations and moment tensor inversion results for the 64 events studied The events and their source parameters are given in Table 1. The locations are from Ito *et al.* (2002) and the KOERI catalogue (http://www.koeri.boun.edu.tr).

4 DISCUSSION

4.1 Tectonic models

The GPS studies and the morphological signature of the NAF show that it changes direction from E–W to WSW to the west of 27.5°E. How the local stress field is influenced by such a change and how the local stress field varies along the Sea of Marmara are investigated using the focal mechanisms shown in Fig. 5 and Table 1. The stress-tensor analysis results yield a similar stress magnitude ratio, $R = 0.5$, for both the eastern and western parts of the Sea of Marmara (Fig. 6). The orientations of the principal stress axes in the eastern part are nearly vertical for σ_2 and nearly horizontal for σ_1 and σ_3. According to Anderson's (1951) theory of faulting this suggests a tectonic regime where strike-slip faulting is dominant (Twiss & Moores 1992, p. 203). This is the case for the eastern part, as observed in Fig. 5, where most of the faults except the Yalova–Cinarcik fault experience strike-slip faulting. The situation is more complicated in the western part. The plunge of the σ_1-axis is the same as for the eastern part, but the azimuth is rotated counter-clockwise by 16°. The minimum misfit error between the observed and predicted *P*- and *T*-axes was 5.8°. Significant biases are also observed in the plunges of the σ_2- and σ_3-axes. While the plunge of the σ_2-axis is close to vertical in the eastern part, it is close to horizontal in the western part. Significant differences are also observed in the plunge of σ_3. The stress field associated with these parameters suggests a

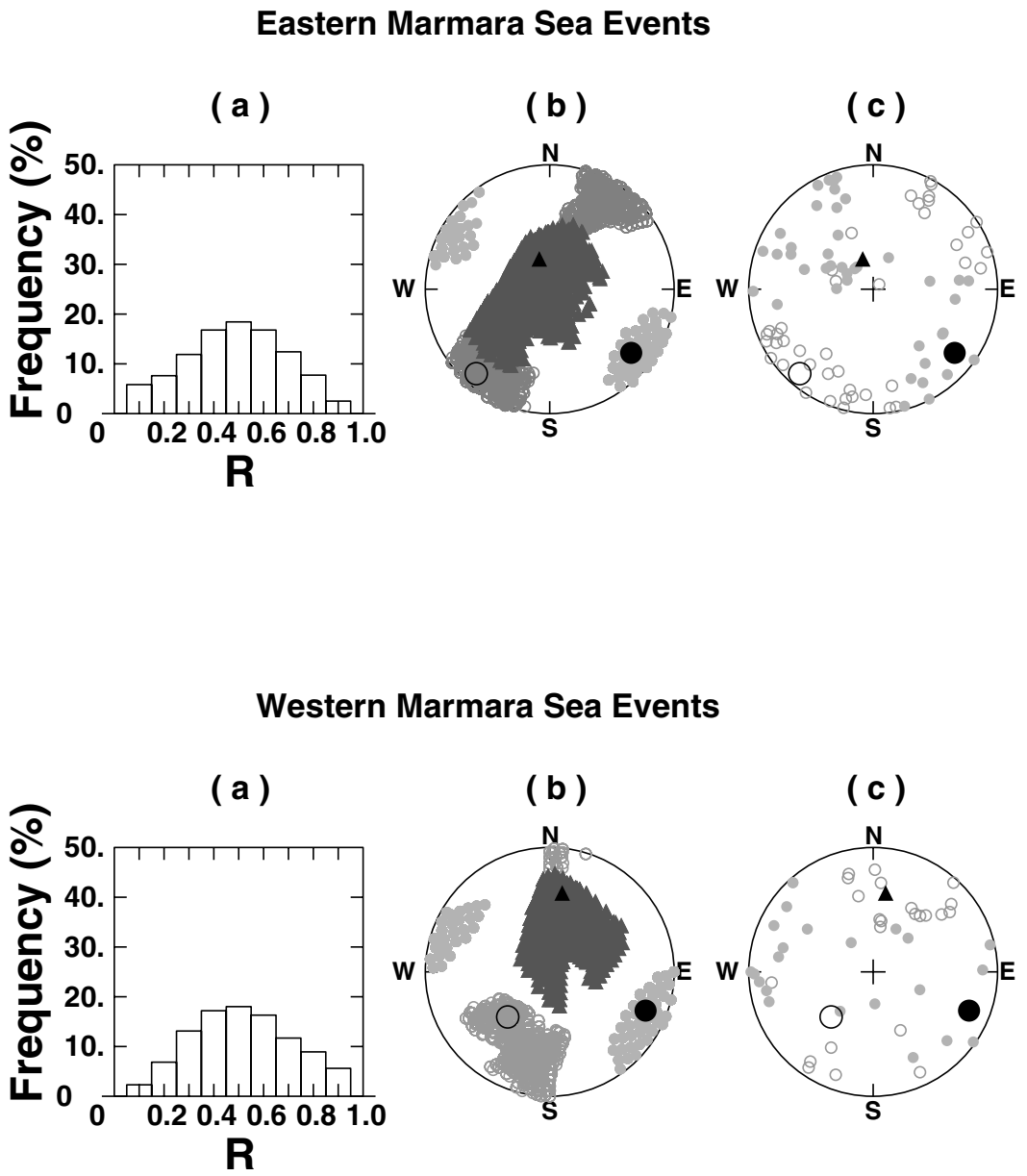

Figure 6. The results of regional stress tensor analysis for the eastern and western parts of the Sea of Marmara, based on the *P*- and *T*-axes of the focal mechanisms given in Fig. 5: (a) the histogram of *R*-values, (b) the distribution of the predicted principal stress axes and their 95 per cent confidence regions and (c) the distribution of the observed *P*- and *T*-axes. In (b), red dots show the azimuth and plunge of the maximum stress axis σ_1, blue circles those of the minimum stress axis σ_3 and green triangles those of the intermediate stress axis σ_2. In (c), red dots show the *P*-axes and blue circles the *T*-axes. Black symbols denote the axes for the best stress model. For both the regions, the best fit was attained for $R = 0.5$ and for the azimuth and plunge pair of (128°, 18°) for σ_1, (19°, 69°) for σ_2 and (221°, 11°) for σ_3, respectively, for the eastern Marmara events and the azimuth and plunge pair of (112°, 18°) for σ_1, (9°, 36°) for σ_2 and (223°, 49°) for σ_3, respectively, for the western part.

transpressive tectonic regime in the western part of the Sea of Marmara, probably resulting from a left step-over of the E–W-trending NAF as it approaches the western coastlines.

The focal mechanisms of the events that occurred in the eastern part of the Sea of Marmara are more homogenous than those of the events that occurred in the western part. From the results shown in Fig. 5 three distinct faulting types are easily identified. The focal mechanism diagrams of the ten events numbered from 33 to 42 and their locations imply a right-lateral strike-slip fault striking NW–SE; this is called the Princes' Island (PI) Fault in Pınar *et al.* (2001). We estimate the length of this fault to be 60 km, taking into account the locations of events 29, 30 and 62 and their mechanisms. This fault was also identified by Okay *et al.* (2000) and Imren *et al.* (2001), who claim that it is the main fault trace. The relation between the fault length and the magnitude of Wells & Coppersmith (1994), $\log L = 0.69\, M_w - 3.22$ (global scale for $M_w = 5.2$–8.1), suggests that this fault has the potential to generate an event of $M_w = 7.2$.

To estimate the present seismic hazard associated with this fault, we follow the next three steps. First, the facts that the previous event on this fault was in 1766 (Ambraseys & Jackson 2000) and

that slip rate in this area is approximately 2 cm yr^{-1} indicate that strain equivalent to a slip of approximately 450 cm has already accumulated on the fault. Secondly, we exploit the relation, $M_o = \mu Au$, where M_o is the seismic moment, μ is the rigidity taken as 3×10^{10} MPa, A is the fault area and u is the displacement. Assuming a 15 km thickness for the seismogenic zone, if this strain were released in a single earthquake it would have a seismic moment of 1.2×10^{20} N m. Finally, using the relation between the seismic moment and the moment magnitude, $M_w = 0.67 \log M_o - 6.0$, we estimate an earthquake magnitude of $M_w = 7.4$ for the Princes' Island fault. These estimates are valid only if the Princes' Island fault is the main fault trace along which the motion between Anatolia and Eurasia is accommodated. On the other hand, Reilinger *et al.* (1997) claim that no more than 60 per cent of the deformation is accommodated along the northern boundary faults, implying a smaller amount of strain accumulation than the above estimation. In addition, Reilinger & McClusky (2001) and Meade *et al.* (2002) analysed dense GPS data acquired in the Sea of Marmara region and came to the conclusion that the NAF trace should be traversing the sea in its central portions rather than along its northern shelves. Thus, we have two possible interpretations of our moment tensor solutions for the events that occurred on the PI fault. In 'Case I', the PI segment is the main fault trace as was recently suggested by Pınar *et al.* (2001), Imren *et al.* (2001) and Okay *et al.* (2000) and in 'Case II', the PI segment is a secondary fault as favoured for the local GPS data (Reilinger & McClusky 2001; Meade *et al.* 2002).

We are now inclined to consider that the PI fault is not the main fault trace but rather that it developed as a secondary fault in a right-lateral strike-slip shear zone, as suggested by our tectonic model for the eastern part, based on the faults identified from the results presented in Fig. 5.

The focal mechanisms numbered from 45 to 55 form a distinct set of events marking out an E–W-striking normal fault. Taking into account the topography the nodal plane dipping north with a small right-lateral strike-slip component should be the fault plane. *The average depth of these earthquakes is approximately 5 km* as shown in Table 1, relatively shallower than the CMT depths of Princes' Island events. Pınar *et al.* (2001) argue the possibility that this fault was ruptured by the 1963 Cınarcık earthquake ($M_s = 6.3$). The locations and the mechanisms of events 56–60 together constitute evidence for a second right-lateral strike-slip fault striking ENE–WSW. Pınar *et al.* (2001) identified this fault from the epicentre distribution of hundreds of earthquakes triggered by the 1999 Izmit event ($M_w = 7.5$). They called it the Yalova–Hersek fault and considered that it might be as much as 50 km long. They also claimed that the fault was not ruptured during the 1999 Izmit earthquake and that the average Coulomb stress increase on the fault resulting from that earthquake is approximately 5 bar.

What is the tectonic significance of these three faults with different fault parameters? Hancock (1985) illustrated the styles of faulting that are likely to occur in a strike-slip deformation zone. Considering the orientation of the maximum (σ_1) and minimum (σ_3) compressive axes inferred in the previous section and Hancock's work, we construct a deformation ellipse for the eastern part of the Sea of Marmara as shown in Fig. 7. Here, Y–Y corresponds to the main fault trace, that is, the Izmit fault segment in Fig. 1. R–R is the Riedel shear zone and corresponds to the PI segment, P–P corresponds to the Yalova–Hersek segment. It is also interesting to note the good correspondence between the extensional faults in the deformation ellipse and the Yalova–Çınarcık normal fault. The R_1–R_1 line in Fig. 7 is a conjugate Riedel shear. The characteristics of R_1 shears are such that they are antithetic to the main fault trace, that is, the sense of motion is opposite to that of the main fault trace and they are oriented at high angles (approximately 70°–80°) to the fault (Twiss & Moores 1992, p. 116). Assuming that the nodal planes striking NNW–SSE are fault planes the locations and the focal mechanism solutions of event nos 43 and 44 suggest that these two events occurred on the conjugate Riedel shears. The rest of the events showing predominantly thrusting or oblique motion with a thrust component correspond to the locations denoted by T (thrust) in the deformation ellipse. Note that the deformation ellipse explains almost all the types of mechanism observed in the eastern part of the Sea of Marmara. This, in turn, implies that the PI, Hersek–Yalova and Yalova–Çınarcık segments are subsidiary shear zones controlled by a larger fault, the orientation of which should be nearly E–W and should extend into the centre of the Sea of Marmara rather than along the northern or southern shelves. This result contradicts the studies of Okay *et al.* (2000), Pınar *et al.* (2001) and Imren *et al.* (2001), according to which the main strand of the NAF turns from E–W to WNW as it enters the sea. Fig. 8(a) illustrates schematically the location of the main strand of NAF and the location of the subsidiary shear zones (based on the locations and mechanisms of the events) formed by the present stress distribution of the principal stress axes and nearly E–W extension of NAF in the eastern part of the Sea of Marmara.

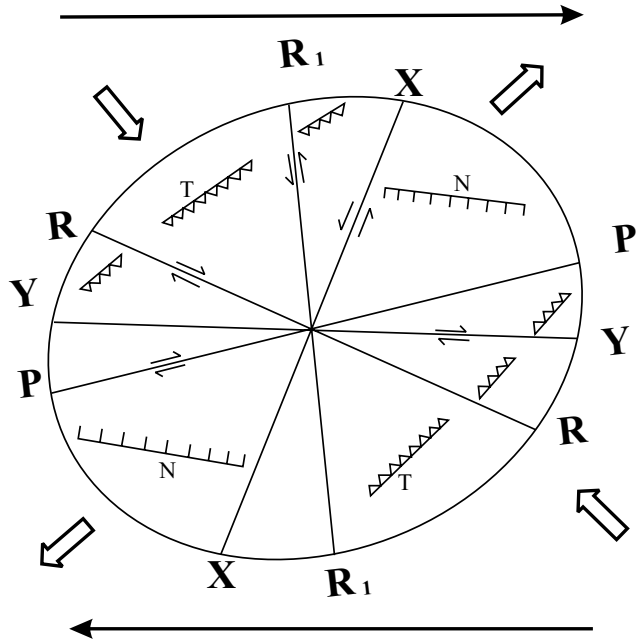

Figure 7. The orientations and sense of motion on subsidiary shear zones associated with a major E–W right-lateral strike-slip fault within a stress field with principal stress axes of NW–SE maximum compression, $\Delta\sigma_1$, and NE–SW minimum compression, σ_3. R–R is a Riedel shear synthetic to the main fault trace (Y–Y), R1–R1 is a conjugate Riedel shear antithetic to the main fault, P–P is also synthetic but compared with the Riedel shear zones it develops at a smaller angle to the main fault. N denotes normal fault and T denotes thrust.

Thus, according to this model, the PI segment is not the main fault. However, a problem remains. How can we explain the Çınarcık basin and the lack of normal faulting? These indicate an extensional tectonic regime. To give a reasonable answer to this problem, we consider the relation between the basin and the dextral PI fault, referring to the study of Zachariasen & Sieh (1995, Fig. 5). They

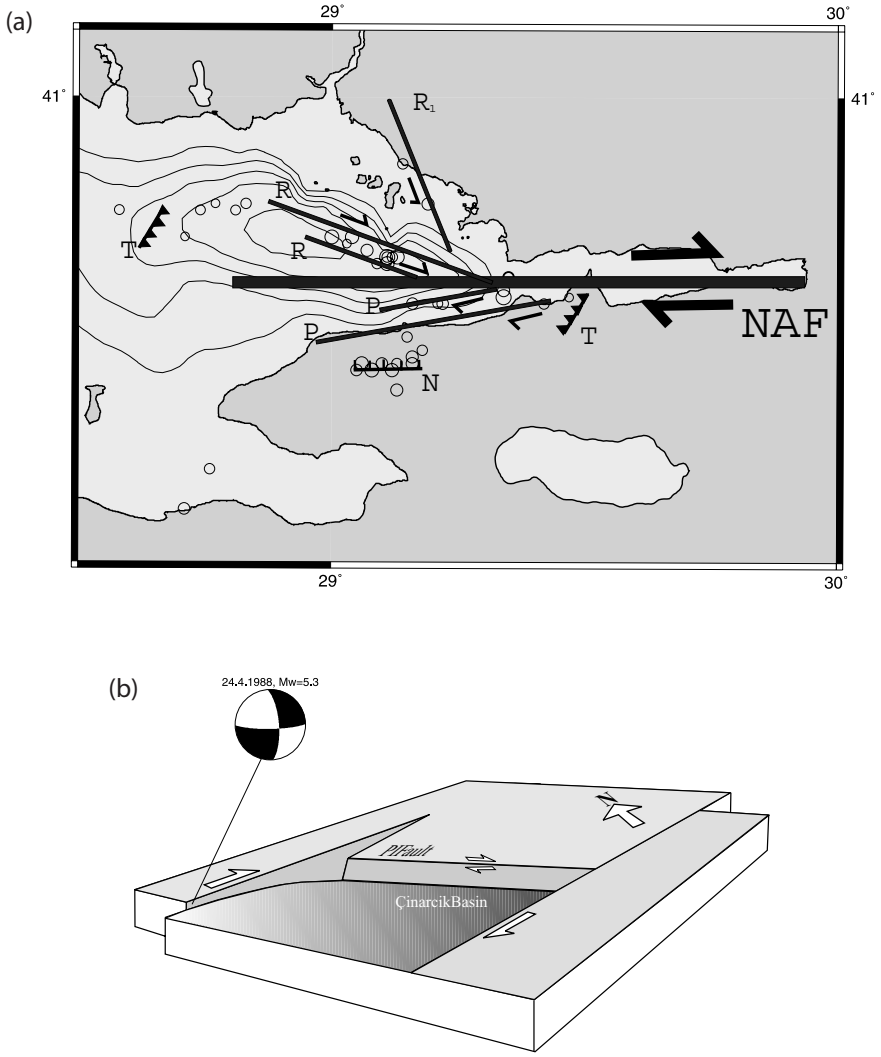

Figure 8. (a) A tectonic model for the eastern part of the Sea of Marmara based on the subsidiary shear zones illustrated in Fig. 7 and the focal mechanism results given in Fig. 5. Contrary to the studies of Imren *et al.* (2001) and Okay *et al.* (2000), the model suggests an E–W continuation of the North Anatolian fault rather than a change of strike or bifurcation as it enters the sea (YÇ, Yalova–Çınarcık fault; YH, Yalova–Hersek fault). (b) Fault configuration in the eastern part of the Sea of Marmara analogous to the Homestead Valley–Emerson Fault step-over in Southern California (Zachariasen & Sieh 1995 , Fig. 5). The figure shows how a step-over on the main fault trace forms a strike-slip duplex with a subsided interior. The Harvard CMT solution for the 1988 April 24 event ($M_w = 5.3$) suggests a location for the E–W-striking main fault zone.

showed how a step-over on the main fault trace forms a strike-slip duplex with a subsided interior. In this sense, the PI segment resembles the Homestead Valley–Emerson Fault step-over in Southern California (Zachariasen & Sieh 1995). In this model, we have the dextral E–W Izmit and WNW–ESE PI faults, and the subsided Çınarcık basin (Fig. 8b). We have two main faults in this model, namely the E–W extension of the Izmit fault in the south of the basin and the trace of the E–W main fault in the north of the step-over. The first is shown in the study of (Siyako *et al.* 2000, Fig. 1c) and the second is implied by the Harvard CMT solution of the 1988 April 24 Marmara Sea event ($M_w = 5.3$), which is likely to have taken place on an E–W fault located in the north of the basin (Fig. 8b). Thus, we conclude that the PI segment is a secondary fault formed as a result of right step-over of the NAF as it enters the Sea of Marmara.

Using the *P*- and *T*-axes of the focal mechanisms of the events located west of 28°E in Fig. 5, we derived the azimuths and plunges of the principal stress axes acting in the western part of the Sea of Marmara. When we compare the azimuth of σ_1 derived for the eastern part with the azimuth derived for the western part, we find a 16° counter-clockwise rotation of the maximum compressive axis, σ_1, in the west. By virtue of this fact, we rotate the deformation ellipse given in Fig. 7 by 16° counter-clockwise to examine the types of faults that may develop in a stress state obtained for the western part of the Sea of Marmara, resulting in the deformation ellipse shown in Fig. 9. Here, Y–Y corresponds to the main fault trace (Ganos fault in Fig. 1) which was subject to rupture during the 1912 Şarköy–Mürefte earthquake ($M_s = 7.4$). R–R is a subsidiary shear zone, the strike of which corresponds very well to the strike slip fault identified by Imren *et al.* (2001). The focal mechanisms of the events numbered 5–16 coincide either with the R_1–R_1 or P–P shears, depending on which of the nodal planes is taken as a fault plane. Also, the locations and the mechanisms of predominantly normal and thrust faulting events 18–20 fit well with the deformation ellipse. Fig. 9 suggests a significant change of strike of the main fault trace from nearly E–W to WSW–ENE, which is confirmed by

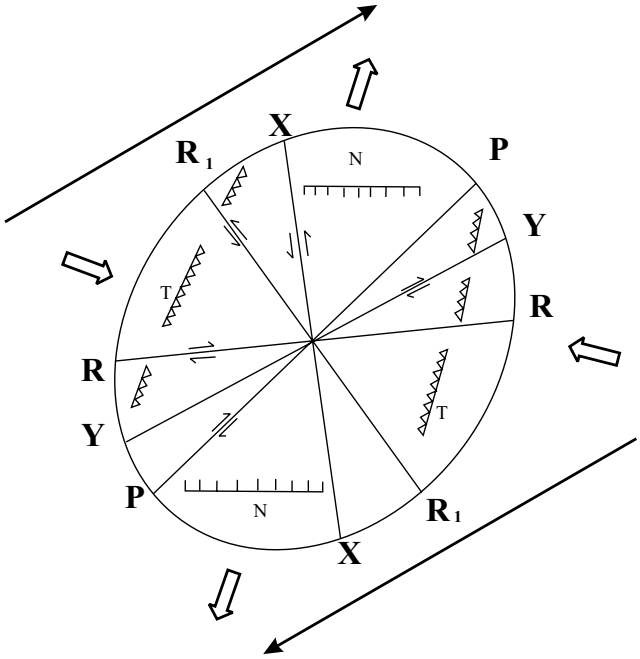

Figure 9. A deformation ellipse for the western part of the Sea of Marmara. The notation is the same as in Fig. 7. 16° counter-clockwise rotation results in the change of strike of NAF from E–W to WSW–ENE, which corresponds to the Ganos fault, ruptured during the 1912 Şarköy–Mürefte earthquake (M_s = 7.4).

GPS studies and the morphological features of NAF. Compared with the eastern part, the focal mechanisms in the western part are more heterogeneous, implying a more heterogeneous stress field, probably resulting both from this sudden change of strike of the NAF and the increasing influence of the N–S extensional tectonic regime acting in the Aegean Sea. The deformation models proposed above for the eastern and western ends of the Sea of Marmara suggest right and left step-over, respectively, of the E–W-trending NAF.

4.2 Stress triggering and implications for seismic hazard

Pınar *et al.* (2001), argued that the main rupture associated with the 1999 Izmit earthquake terminated just to the east of the Hersek delta and that the events occurring to the west of the Hersek delta were triggered by static stress increase. Then, it would have been interesting to investigate how the subsidiary shear zones that we identified in the eastern part of the Sea of Marmara reacted to this stress transfer. From Table 1 we see that all the events (except no 33) that form the Riedel shear zone in Fig. 7 occurred within 24 h of the main shock. However, events 56–60 and 63, which form the *P* shear zone in Fig. 7, occurred several days after the main shock, and even the $M_w > 4$ ones occurred several months later. At first glance, this fact suggests that the *R* shears are activated more easily than the *P* shears. Pınar *et al.* (2001) estimated approximately 0.1 and 0.5 MPa stress increase on the *R* and *P* shear zones, respectively. Both of the shear zones are optimally oriented right-lateral strike-slip faults determined by the effect of the regional stress tensor and the main rupture zone of the 1999 Izmit earthquake. Thus, high seismic activity was triggered on them. However, taking into account the distance of the shear zones to the site of termination of the rupture (east of the Hersek delta) of the 1999 main shock, we can see that the $M_w > 4$ events occurred within several hours of the main shock on the *R* shears and several months later on the *P* shear zones.

One possible explanation for the triggering delay comes from the study of Tchalenko (1970) who conducted a laboratory study to investigate the rupture patterns that develop in the vicinity of a major fault zone prior to failure. His experiment clearly shows that minor slip is required to activate *R* zones and somewhat larger slip is necessary to activate the *P* shear zones. Adapting these results to our model, we can conclude that 0.1 MPa stress transfer to the *R* shear zone was sufficient to trigger the $M > 4$ events there, but 0.5 MPa stress transfer on the *P* shear zone was sufficient only to trigger microactivity. For the $M > 4$ events on the *P* shear zone, additional stress transfer was necessary and it took a couple of months for additional stress to be provided by post-seismic slip as observed by Reilinger *et al.* (2000). An alternative explanation for the time of triggering is the level of stress on the shear zones prior to the main shock.

In fact, we know neither the stress values on the *R* and *P* shear zones just before the Izmit earthquake nor the strength of the *R* and *P* shear zones. If we assume similar strengths for the *R* and *P* shear zones and also assume that the $M > 4$ events were activated on account of the higher stress level present just prior to the main shock, we can speculate concerning the previous event that occurred on the *R* and *P* shear zones. Because of these assumptions, the events that

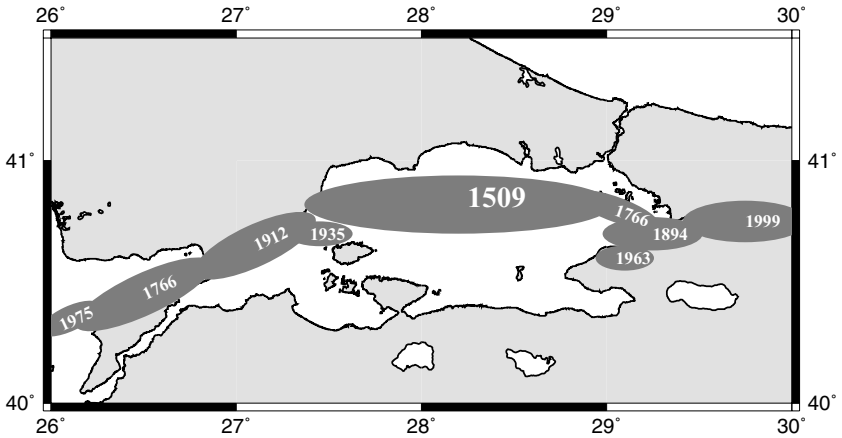

Figure 10. The locations of the $M > 6$ events occurred along the North Anatolian fault zone in the Sea of Marmara, Gulf of Izmit and Dardaneles during the last 500 yr (Ambraseys & Jackson 2000). The size of the ellipses is proportional to the event size.

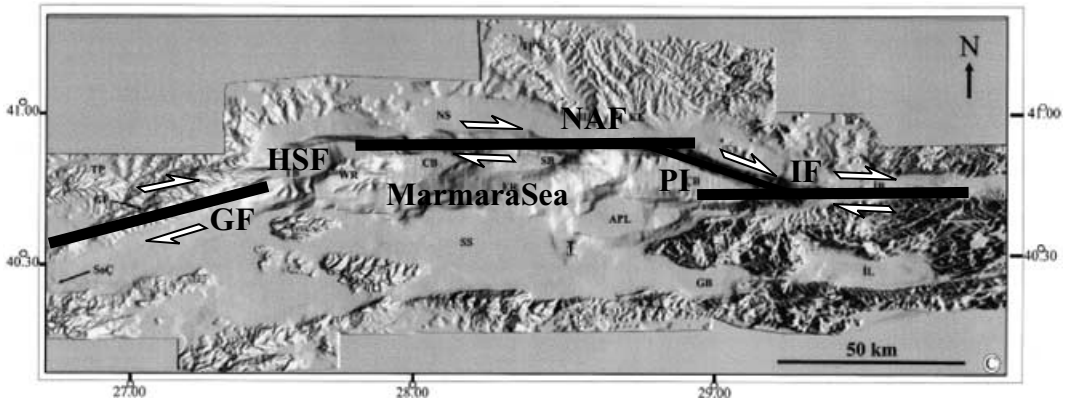

Figure 11. Fault model showing the segmentation and right and left step-over of the NAF, in eastern and western parts of the Sea of Marmara, respectively. The morphological map of the Sea bottom is prepared by Gazioğlu *et al.* (2002). The abbreviations are as follows: GF, Ganos fault; NAF, North Anatolian fault; IF, Izmit fault; PI, Princes' Island fault; HSF, heterogenious stress field region. The arrows indicate the sense of motion.

occurred on the PI segments required a higher stress level, implying longer stress accumulation times. This result favours the study of Ambraseys & Jackson (2000) who claimed that the PI segment was ruptured in 1766 May by an event of $M_s = 7.1$ and that the most recent moment release on the Yalova–Hersek segment occurred in 1894.

The major points of our models are: (1) the PI is not a main fault trace; (2) the NAF does not bifurcate as it enters the Sea of Marmara, but terminates south of the Çınarcık basin and then jumps to the north of it and continues westward nearly E–W; (3) since there is no branching of the NAF in the eastern Marmara there should not be strain partitioning and the entire motion along the NAF is accommodated by the single westward-continuing strand. Thus, taking into account the 1935 western Marmara Sea event ($M_s = 6.4$), which occurred in the western part, and 1963 Cinarcik event ($M_s = 6.3$), and also the study of Rockwell *et al.* (2001), which provided some evidence that the second major event of 1766 occurred to the west of the 1912 event, we conclude that no major event took place beneath the sea since 1509, when the greatest known event occurred (Fig. 10). This conclusion, along with the GPS studies, suggests that unless creeping is taking place along the main fault trace, the strain already accumulated is capable of producing an event as large as $M_w = 7.9$.

5 CONCLUSIONS

Our conclusions are as follows.

(1) The moment tensor solutions of the Marmara Sea events show that the stress field in the eastern part is homogenous, but in the western part is very heterogeneous. The heterogeneity may result from a change in the strike of NAF from nearly E–W to WSW–ENE.

(2) The azimuth of the maximum compressive principal stress axis, σ_1, for the eastern and western part of the Sea of Marmara is 128° and 112°, respectively, suggesting a counter-clockwise rotation of the stress field. The σ_2-axis is close to vertical in the eastern part (shear tectonic regime), whereas its plunge in the western part is 36°, suggesting a transpressive tectonic regime.

(3) The locations and mechanisms of the eastern Marmara Sea events identify several secondary faults. The orientation and sense of motion on these faults are explained by a simple tectonic model that requires a nearly E–W-striking main fault trace, namely the NAF. Also, the location and sense of motion on the secondary faults are successfully predicted by *R* and *P* shears and their conjugates.

(4) We propose a tectonic model for the eastern and western ends of the Sea of Marmara that requires right and left step-over, respectively, of the E–W-trending NAF (Fig. 11).

(5) Taking into account the historical seismicity, our model indicates that no major event has occurred beneath the Sea of Marmara since 1509. The region between the PI segment and the Ganos fault ruptured by the 1912 Mürefte earthquake is identified as a possible gap and if it is to be filled by a single event, it corresponds to an event of $M_w = 7.9$.

ACKNOWLEDGMENTS

We thank the staff of the Seismological Laboratory of Kandilli Observatory and Earthquake Research Institute for the broad-band data used in this study. We benefited from the comments raised by Gene Ichinose, an anonymous referee and J. Russ Evans who also improved the English in the manuscript. This work was supported by the Research Fund of the University of Istanbul through project numbers B-1317/15102001 and 1497/28082000.

REFERENCES

Ambraseys, N.N. & Jackson, J.A., 2000. Seismicity of the Sea of Marmara (Turkey) since 1500, *Geophys. J. Int.,* **141,** F1–F6.

Anderson, E.M., 1951. *The Dynamics of Faulting*, 2nd edn, Oliver and Boyd, Edinburgh.

Barka, A.A. & Kadinsky-Cade, K., 1988. Strike-slip fault geometry in Turkey and its influence on earthquake activity, *Tectonics,* **7,** 663–684.

Christova, C. & Tsapanos, T., 2000. Depth distribution of stresses in the Hokkaido Wadati–Benioff zone as deduced by inversion of earthquake focal mechanisms, *J. Geodyn.,* **30,** 557–573.

Delouis, B. & Legrand, D., 1999. Focal mechanism determination and identification of the fault plane of earthquakes using only one or two near-source seismic recordings, *Bull. seism. Soc. Am.,* **89,** 1558–1574.

Dreger, D.S. & Helmberger, D., 1991. Source parameters of the Sierra Madre earthquake from regional and local body waves, *Geophys. Res. Lett.,* **18,** 2015–2018.

Dreger, D. & Helmberger, D., 1993. Determination of source parameters at regional distances with single station or sparse network data, *Bull. seism. Soc. Am.,* **98,** 8107–8125.

Dreger, D. & Savage, B., 1999. Aftershocks of the 1952 Kern County, California, Earthquake Sequence, *Bull. seism. Soc. Am.,* **89,** 1094–1108.

Fan, G. & Wallace, T., 1991. The determination of source parameters for small earthquakes from a single, very broadband seismic station, *Geophys. Res. Lett.,* **18,** 1385–1388.

Gazioğlu, C., Gökaşan, E., Algan, O., Yücel, Z., Tok, B. & Doğan, E., 2002. Morphological features of the Marmara Sea from multibeam data, *Marine Geol.,* **190,** 397–420.

Gephart, J.W., 1985. Principal stress directions and the ambiguity in fault plane identification from focal mechanisms, *Bull. seism. Soc. Am.,* **75,** 621–625.

Gephart, J.W., 1990. FMSI: a Fortran program for inverting fault/slickenside and earthquake focal mechanism data to obtain the regional stress tensor, *Comp. Geosci.,* **16,** 953–989.

Gephart, J.W. & Forsyth, D.W., 1984. An improved method for determining the regional stress tensor using earthquake focal mechanism data: application to the San Fernando earthquake sequence, *J. geophys. Res.,* **89,** 9305–9320.

Gürbüz, C. *et al.*, 2000. The seismotectonics of the Marmara region (Turkey): results from a microseismic experiment, *Tectonophysics,* **316,** 1–17.

Hancock, P.L., 1985. Brittle microtectonics: principles and practice, *J. struc. Geol.,* **7,** 437–457.

Imren, C., Le Pichon, X., Rangin, C., Demirbag, E., Ecevitoğlu, B. & Görür, N., 2001. The North Anatolian Fault within the Sea of Marmara: a new interpretation based on multichannel seismic and multibeam bathymetry data, *Earth planet. Sci. Lett.,* **186,** 143–158.

Ito, A. *et al.*, 2002. Aftershock activity of 1999 Izmit earthquake, Turkey, revealed from microearthquake observations, *Bull. seism. Soc. Am.,* **92,** 418–427.

Kahle, H.-G., Cocard, M., Peter, Y., Geiger, A., Reilinger, R., Barka, A. & Veis, G., 2000. GPS-derived strain rate field within the boundary zones of the Eurasian, African, and Arabian plates, *J. geophys. Res.,* **105,** 23 353–23 370.

Kalafat, D., 1998. Anadolunun tektonik yapılarının deprem mekanizmaları açısından irdelenmesi, *Deprem Araştırma Bülteni,* **77,** 1–217.

Kalafat, D., Gürbüz, C. & Üçer, S.B., 1987. Batı Türkiyede kabuk ve üst manto yapısının arastırılması, *Deprem Arastırma Bülteni,* **14,** 43–64.

Kim, S.G. & Kraeva, N., 1999. Source parameter determination of local earthquakes in Korea using moment tensor inversion of single station data, *Bull. seism. Soc. Am.,* **89,** 1077–1082.

Kohketsu, K., 1985. The extended reflectivity method for synthetic near-field seismograms, *J. Phys. Earth,* **33,** 121–131.

Kuge, K., 1999. Automated determination of earthquake source parameters using broadband strong-motion waveform data, *EOS, Trans. Am. geophys. Un.,* **80,** F661.

Legrand, D. & Delouis, B., 1999. Determination of the fault plane using a single near-field seismic station with a finite-dimension source model, *Geophys. J. Int.,* **138,** 801–808.

Legrand, D., Kaneshima, S. & Kawakatsu, H., 2000. Moment tensor analysis of near-field broadband waveforms observed at Aso Volcano, Japan, *J. volc. geoth. Res.,* **101,** 155–169.

McClusky, S. *et al.*, 2000. Global Positioning System constraints in plate kinematics and dynamics in the eastern Mediterranean and Caucasus, *J. geophys. Res.,* **105,** 5695–5719.

Meade, B.J., Hager, B.H., McClusky, S.C., Reilinger, R.E., Ergintav, S., Lenk, O., Barka, A. & Özener, H., 2002. Estimates of seismic potential in the Marmara Sea region from block models of secular deformation constraints by GPS measurements, *Bull. seism. Soc. Am.,* **92,** 216–229.

Okay, A., Demirbag, E., Kurt, H., Okay, N. & Kuşçu, I., 1999. An active, deep marine strike-slip basin along the North Anatolian fault in Turkey, *Tectonics,* **18,** 129–147.

Okay, A.I., Kaşlılar-Özcan, A., Imren, C., Boztepe-Güney, A., Demirbağ, E. & Kuşçu, I., 2000. Active faults and evolving strike-slip basins in the Marmara Sea, northwest Turkey: a multichannel seismic reflection study, *Tectonophysics,* **321,** 189–218.

Örgülü, G. & Aktar, M., 2001. Regional moment tensor inversion for strong aftershocks of the August 17, 1999 Izmit Earthquake ($M_w = 7.4$), *Geophys. Res. Lett.,* **28,** 371–374.

Parke, J.R. *et al.*, 1999. Active faults in the Sea of Marmara, western Turkey, imaged by seismic reflection profiles, *Terra Nova,* **11,** 223–227.

Parsons, T., Toda, S., Stein, R.S., Barka, A.A. & Dietrich, J.H., 2000. Heightened odds of large earthquakes near Istanbul: an interaction-based probability calculation, *Science,* **288,** 573–576.

Pınar, A., Honkura, Y. & Kuge, K., 2001. Seismic activity triggered by the 1999 Izmit earthquake and its implications for the assessment of future seismic risk, *Geophys. J. Int.,* **146,** F1–F7.

Reilinger, R. & McClusky, S., 2001. GPS constraints on block motions and deformation in western Turkey and the Aegean: implications for earthquake hazards, in *Seismotectonics of the North-Western Anatolia–Aegean and Recent Turkish Earthquakes*, pp. 14–20, ed. Taymaz, T., ITU, Istanbul.

Reilinger, R.E. *et al.*, 1997. Global Positioning System measurements of present-day crustal movements in the Arabia–Africa–Eurasia plate collision zone, *J. geophys. Res.,* **102,** 9983–9999.

Reilinger, R.E. *et al.*, 2000. Coseismic and postseismic fault slip for the 17 August 1999, $M = 7.5$, Ismit, Turkey earthquake, *Science,* **289,** 1519–1524.

Ritsema, J. & Lay, T., 1995. Long-period regional wave moment tensor inversion for earthquakes in the western United States, *J. geophys. Res.,* **100,** 9853–9864.

Rockwell, T., Barka, A., Dawson, T., Akyüz, S. & Thorup, K., 2001. Paleoseismology of the Gaziköy–Saros segment of the North Anatolian fault, northwestern Turkey: comparison of the historical and paleoseismic records, implications of regional seismic hazard, and models of earthquake recurrence, *J. Seism.,* **5,** 433–448.

Singh, S.K., Pacheco, J., Courboulex, F. & Novelo, D.A., 1997. Source parameters of the Pinotepa Nacional, Mexico, earthquake of 27 March, 1996 ($M_w = 5.4$) estimated from near-field recordings of a single station, *J. Seism.,* **1,** 39–45.

Siyako, M., Tanış, T. & Şaroğlu, F., 2000. The active fault geometry of the Sea of Marmara: an interpetation of the fault map of TPAO, *TUBITAK,* **388,** 66–71 (in Turkish).

Slancova, A., Spicak, A., Hanus, V. & Vanek, J., 2000. Delimination of domains with uniform stress in the subducted Nazca plate, *Tectonophysics,* **319,** 339–364.

Smith, A.D. *et al.*, 1995. High-resolution seismic profiling in the Sea of Marmara (northwest Turkey): Late Quaternary sedimentation and sea-level changes, *Geol. Soc. Am. Bull.,* **107,** 923–936.

Straub, C., Kahle, H.G. & Schindler, C., 1997. GPS and geological estimates of the tectonic activity in the Marmara Sea region, NW Anatolia, *J. geophys. Res.,* **102,** 27 587–27 601.

Tchalenko, J., 1970. Similarity between shear zones of different magnitude, *Geol. Soc. Am. Bull.,* **81,** 1625–1640.

Twiss, R.J. & Moores, E.M., 1992. *Structural Geology,* Freeman, New York, p. 532.

Wells, D.L. & Coppersmith, K.J., 1994. New empirical relations among magnitude, rupture length, rupture area, and surface displacement, *Bull. seism. Soc. Am.,* **84,** 974–1002.

Wong, H.K., Ludmann, T., Uluğ, A. & Görür, N., 1995. The sea of Marmara: a plate boundary sea in an escape tectonic regime, *Tectonophysics,* **244,** 231–250.

Zachariasen, J. & Sieh, K., 1995. The transfer of slip between, *en echelon* strike-slip faults: a case study from the 1992 Landers earthquake, southern California, *J. geophys. Res.,* **100,** 15 281–15 301.